A comparison of several artificial neural network classifiers for CT images of hardwood logs

Daniel L. Schmoldt[a], Jing He[b], and A. Lynn Abbott[c]

[a]US Forest Service, Brooks Center, Virginia Tech, Blacksburg VA 24061-0503
[b]Communication Technology Group, COMSAT LAB, 22300 COMSAT Drive, Clarksburg MD 20871
[c]Bradley Department of Electrical Engineering, Virginia Tech, Blacksburg VA 24061-0111

ABSTRACT

Knowledge of internal log defects, obtained by scanning, is critical to efficiency improvements for future hardwood sawmills. Nevertheless, before computed tomography (CT) scanning can be applied in industrial operations, we need to automatically interpret scan information so that it can provide the saw operator with the information necessary to make proper sawing decisions. Our current approach to automatically label features in CT images of hardwood logs classifies each pixel individually using a back-propagation artificial neural network (ANN) and feature vectors that include a small, local neighborhood of pixels and the distance of the target pixel to the center of the log. Initially, this ANN was able to classify clear wood, bark, decay, knots, and voids in CT images of two species of oak with 95% pixel-wise accuracy. Recently we have investigated other ANN classifiers, comparing 2-D versus 3-D neighborhoods and species-dependent (single species) versus species-independent (multiple species) classifiers using oak, yellow poplar, and cherry CT images. When considered individually, the resulting species-dependent classifiers yield similar levels of accuracy (96-98%). 3-D neighborhoods work better for multiple-species classifiers and 2-D is better for single-species. Under certain conditions there is no statistical difference in accuracy between single- and multiple-species classifiers, suggesting that a multiple-species classifier can be applied broadly with high accuracy.

Keywords: industrial inspection, segmentation, computed tomography, image analysis, wood processing, lumber.

1. INTRODUCTION

The manufacture of furniture, cabinets, flooring, millwork, and molding, along with hardwood exports, accounts for most of the high- and medium-grade hardwood lumber consumption in the U.S. Because the value of hardwood lumber is inversely proportional to the quantity and size of defects, each log must be sawn to minimize the defects in the resulting boards. Traditionally, the sawyer chooses a sawing strategy by visually examining the exterior of a log and dynamically adjusting the cutting face as sawing exposes the log interior. This type of sawing is "information limited" in the sense that the sawyer only has knowledge of external indicators of internal features (e.g. defects). Developing nondestructive sensing and analysis methods that can accurately detect and characterize interior defects is critical to future efficiency improvements for sawmills[1].

Studies have demonstrated potential value gains of 11%,[2] 10%,[3] 14%,[4] and 21%[5,6] that can be achieved by sawing logs under different log orientations and using different sawing methods. A tacit assumption for eventual application of internal scanning to log sawing is that knowledge of internal defects will lead to choosing the best sawing position and method, and therefore will allow mills to realize these potential value gains. Log breakdown in this scenario is "fully informed", where the sawyer has knowledge about internal feature size, type, and location. CT scanning has been investigated[7-22] as providing that internal feature information. However, because CT scanner design and development has focused on medical applications, an industrial CT scanner for hardwood log processing does not exist.[21] While we are actively pursuing industrial scanner development, we are also developing the necessary image interpretation software to automatically recognize internal log features and to present this information to the sawyer in a useful manner.

Early work on automatically labeling internal log defects established the feasibility of utilizing CT images for this purpose. These researchers employed a variety of methods to segment different regions of a CT image and then to interpret, or label, those segmented regions. Often, image segmentation methods are based on threshold values derived from image

Further author information —
D.L.S. (correspondence): schmoldt@vt.edu; http://www.se4702.forprod.vt.edu/
J.H.: hej@comsat.com
A.L.A.: abbott@ee.vt.edu

histograms.[22-24] Texture-based techniques have been applied only to defect labeling,[25,26] and not to segmentation. Knowledge-based classification,[27,28] shape examination,[23,25] and morphological operations[23] have also been used to label defects.

While these efforts have demonstrated feasibility, they have some serious limitations. First, reports of defect labeling accuracy are often either anecdotal, based on success in a training set, or based on a single test set. No statistically valid estimates of labeling accuracy can be found in the literature. Second, there has been no effort to assess or to achieve real-time operability of the developed algorithms. Third, texture information is intrinsic to human differentiation of regions in CT images (i.e., image segmentation), and automated recognition algorithms should exploit this fact for computer-based processing.

Recent work by us[29,30] has demonstrated highly accurate labeling of log defects in CT imagery. In contrast to the previous global approaches that separate the tasks of segmentation and region labeling, this approach operates using local, pixel neighborhoods primarily, and effectively combines segmentation and labeling into a single classification step. A feed-forward artificial neural network (ANN) has been trained to accept CT values from a small 2-dimensional (2-D) or 3-dimensional (3-D) neighborhood about the target pixel, and then assigns to each pixel a particular class label. In order to accommodate different types of hardwoods, a histogram-based preprocessing step normalizes CT density values prior to ANN classification. Morphological postprocessing is used to refine the shapes of detected image regions. This approach avoids the limitations of previous approaches, that is, accuracy can be evaluated quantitatively, defect labeling can be accomplished in real time, and texture information is utilized in the segmentation-classification step.

Accuracy achieved by this classification approach is very high (95%) at the pixel level.[30] This previous work, however, used 2 species of oak only, and processed 3-D neighborhoods almost exclusively. The current study extends that work to look at the interaction of neighborhood dimensionally (2-D vs. 3-D) and single- vs. multiple-species classifiers, with respect to their impact on classifier accuracy. The issue that we sought to resolve here is whether we could develop *species-independent* classifiers of high accuracy using our ANN, local-neighborhood approach.

2. NEURAL NET CLASSIFIERS

We have developed species-dependent classifiers and species-independent classifiers for different neighborhoods in CT images. Both 2-D and 3-D neighborhoods have been considered. All of these classifiers contain the same modules, which are: (1) a preprocessing module, (2) an ANN-based classifier, and (3) a post-processing module. The preprocessing module separates wood from background and internal voids, and normalizes the CT density values. The ANN classifier labels each pixel of the image. The post-processing step removes some of the spurious misclassifications. The major difference between the various classifiers is that they are trained with different types of input features and have different sets of ANN weights.

2.1 The Preprocessing Module

2.1.1 Background Segmentation

Background segmentation, which separates the wood region (foreground) from the background and internal voids, is the first objective of the preprocessing module. This step eliminates portions of the image from further analysis which, in turn, simplifies the classification procedure and decrease the classification time. Background thresholding can be accomplished either statically or dynamically. This research applies Otsu's dynamic thresholding method.[31] It has previously demonstrated effectiveness for segmenting CT images of hardwood logs.[29]

Otsu's method assumes a bimodal distribution, in which a threshold t is selected for the histogram $h(i)$ to minimizes the weighted within-mode variances (or, alternatively, maximizes the weighted between-mode variances) When using this thresholding method directly, however, decay in CT images was found to be categorized with background because the presence of decay in an image creates a trimodal histogram. To avoid this problem, a weighting function $w(i)$ is applied to the original image histogram before applying Otsu's method. This weighting function is given by

$$w(i) = 1 - \exp\left[-\left(\frac{i - \frac{x_{cw}}{2}}{b}\right)^2\right], \qquad (1)$$

where i is the CT number, b is set to 2047 (the largest possible CT value in 11-bit data), and x_{cw} is the value of the clear wood peak in the histogram. Then the best threshold is determined by applying Otsu's method to the new histogram function, $h'(i) = h(i) \quad w(i)$. After thresholding the original CT image, the background region is set to zero, and these pixels are ignored in subsequent processing steps. The original CT values are not modified in this step.

2.1.2 Normalization

Normalizing CT image values is the second objective of the preprocessing module. The values in CT images are directly related to the density of the object. Because different species and different logs vary in densities, somewhat different ranges of CT values can result. Histogram normalization translates the original CT image values into new values without disturbing the invariant associations that internal log features have with particular regions of the CT histogram. These associations seem to be, in our experience, consistent across many different species of logs in the green state (i.e., freshly cut).

The transformation we developed is:

$$x_{norm} = \frac{1}{x_0}\left[x_0 + \frac{x_s - x_{cw}}{1 + \exp\left(\alpha\left(\frac{x_{cw}}{2} - x_0\right)\right)}\right], \tag{2}$$

where x_0 is the original CT value, x_{norm} is the normalized value, x_{cw} is the original CT value of the clear wood peak, x_s is an arbitrarily selected anchor value that is greater than the CT value of the clear wood peak. The quantity α is a constant that determines the steepness of the curve and has been set to $10/x_{cw}$. After histogram normalization, the new value of the clear wood peak in an image histogram is approximately 1.0. This translation also stretches the histogram so that mid-histogram features, such as decay, are not compressed into the clear wood portion of the histogram. Normalized CT values for each pixel are used directly by the ANN classifiers.

1.2 ANN Classifiers

The ANN classifier is the seminal part of this classification system. back-propagation neural networks were chosen because their documented effectiveness for pattern-matching problems, and their relative ease of use. Using an ANN, each non-background pixel is labeled. This section describes the procedure for generating a classifier, which includes extracting the input features for classification from the CT images and constructing the neural networks for 2-dimensional and 3-dimensional analysis.

1.2.1 Feature Extraction

Selecting useful features for an ANN is extremely important because they determine how well the classify learns and consequently how it will perform in the future. In this work, the features of each pixel that were extracted from a CT image are the histogram-normalized values of the pixels. These pixels belong to the neighborhood of the pixel under consideration (the target pixel). For 2-D analysis, a pixel's neighborhood contains the pixels within a 5×5 window; for 3-D analysis, its neighborhood contains the pixels within a $3 \times 3 \times 3$ window, i.e. including 3×3 windows from adjacent CT images. Additionally, because some defects, such as splits, are near to the center, and some of them, such as bark and sapwood, are close to the outside edge of the log, the distance from the center of the log to the target pixel is also used as a feature. This distance measure contains contextual (or global) information that can improve classification. The neighborhood of a pixel under consideration for 2-D and 3-D analysis is shown in Figure 1.

Because the 2-dimensional classifiers use a 5×5 window, the features are defined as

$$F(x, y) = \begin{cases} N_{i,2D}(x, y) & i = 1...25 \\ r_i & i = 26 \end{cases}. \tag{3}$$

The 3-dimensional classifiers use a $3 \times 3 \times 3$ window, the features of each pixel are defined as

$$F(x, y) = \begin{cases} N_{i,3D}(x, y) & i = 1...27 \\ r_i & i = 28 \end{cases} . \quad (4)$$

In both (3) and (4), i is the feature number, $F(x, y)$ is the network input feature vector for the target pixel at (x, y), and $N_i(x, y)$, $1 \le i \le n$, is the neighborhood vector of the pixel for neighborhoods of size n. Given a pixel, there are n=25 items in its 2-D neighborhood vector $N_i(x, y)$, and n=27 in its 3-D neighborhood vector. These items are the normalized values of the corresponding pixels. The 26th feature (or 28th, for 3-D) is the radial distance. So the total number of features for each target pixel for 2-D analysis is 26, and for 3-D analysis, the total number is 28.

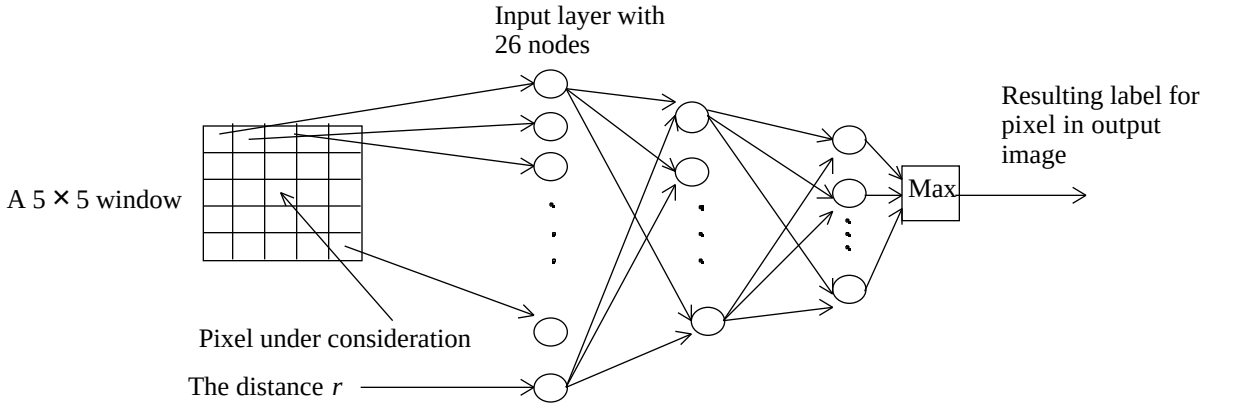

(a)

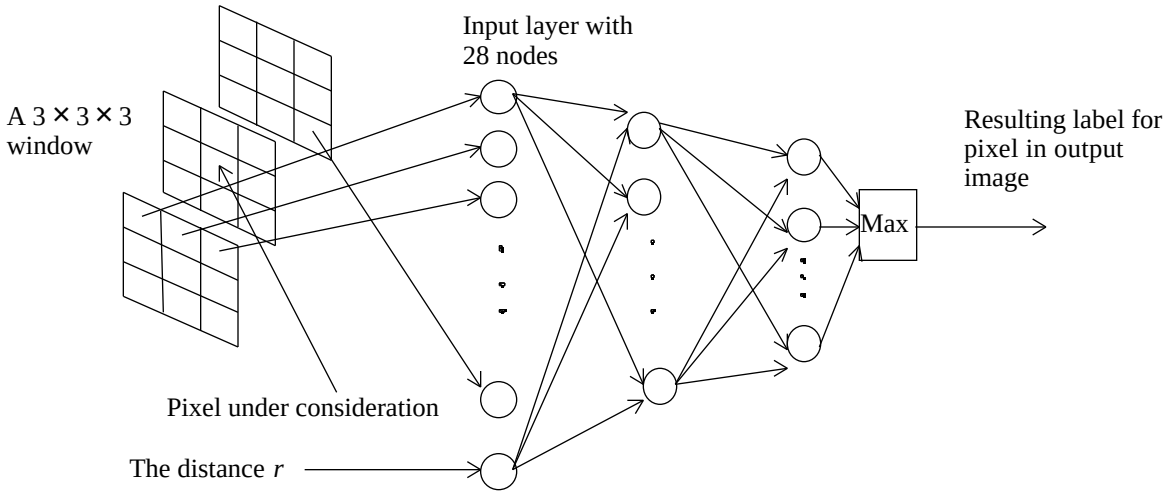

(b)

Figure 1. ANNs containing a 2-D window (a) and a 3-D window (b) illustrate the network topology and relationship of input images to output classifications. The top left pixel in (a) is the input of the first node in the 2-D ANN, while the top left pixel in the previous slice (b) is mapped to the input for the first input node of the 3-D ANN. The distance r is the last input to the ANN in both cases.

1.1.2 Topology

The topology of a neural network has an effect on the speed of convergence during training, and on the accuracy of the classification. Based on prior results[29], the number of hidden nodes was chosen to be 12. The number of output nodes for the ANNs differed, however. In different families of species-dependent and species-independent classifiers, there are different defects to be labeled. For example, red oak classifiers detect five classes: clear wood, knots, bark, splits, and decay. Yellow

poplar and red oak combined classifiers identify six classes: heartwood, knots, bark, splits, decay, and yellow-poplar sapwood. In 2-D classifiers the topology is 26-12-5 or 26-12-6, which means that the structure of the neural network has 26 input nodes, 12 hidden nodes, and 5 or 6 output nodes. In 3-dimensional classifiers the topology is 28-12-5 or 28-12-6, which has a similar interpretation.

1.3 Post-processing

Because classification features are based primarily on local neighborhoods, spurious misclassifications tend to occur at isolated points. A post-processing module is used to remove these small regions, and therefore improve overall system performance. The module includes two mathematical morphological operations: erosion and dilation.

After passing though an ANN classifier, a CT image is labeled and treated as a gray-level image. Then the image is post-processed by the morphological operations of erosion followed by dilation using a 5-point structuring element. In a CT image, splits appear close to the center of a log image, and their appearance after classification is a narrow line. If a split is post-processed, it is often deleted by the erosion operation. Hence, for all classifiers in our study, an entire image is not post-processed, only the outer regions of the log are post-processed. The range of the post-processed region of an image is currently selected manually. Each pixel whose distance r is greater than 0.75 times the ideal log radius is chosen to be post-processed. This approach deletes misclassified small areas—which occur mostly near the outer edges of the log—as well as retains important information (like splits) near the center of the log.

1.4 Training and Testing

An entire training/testing set for one hardwood species consists of approximately 1000 samples. 10-fold cross validation was used to evaluate the accuracy of each classifier. This means that the training set is randomly divided into 10 mutually exclusive test partitions of approximately equal size. For each of the 10 stages of training, one partition is designated as the test set, and the remaining samples in other partitions are used to train the neural network. In successive stages, different partitions are used for testing and the remaining samples are used for training. The average classification accuracy over all 10 stages of training is reported as the cross-validated classification accuracy.

In this work, all the ANNs were trained using the delta rule, which is a learning rule that specifies how connection weights are changed during the learning process. Momentum and learning rate parameters affect the operation of the learning rule. In particular, they affect the speed of convergence of the ANN. With a small learning rate, the neural network converges very slowly. A momentum term is added to the delta rule to solve this problem. This momentum term accelerates learning by increasing weight changes when they are repeatedly in the same direction. Based on Li's results,[29] a small learning rate 0.1 and a medium momentum term 0.6 were selected as the learning parameters for all ANN training of hardwood log CT images. Random values were assigned to the initial weights for each network training session.

3. EXPERIMENTAL DESIGN

As noted above, 1000 samples were taken from each of the species: red oak, yellow poplar, and black cherry. The percentages of these samples for each feature type across the different species appear in Table 1. Both red oak and yellow poplar images have pixel resolution $2.5\times2.5\times2.5$ mm^3. Whereas, the cherry log images were generated by a different scanner at a different resolution, approx. $0.95\times0.95\times0.95$ mm^3. Because image texture differs at these different resolutions we could not combine data across resolutions for multiple-species classifier development. Consequently, $3\times3\times3$ neighborhoods in the 512×512 cherry images (cherry_512) were combined to produce new images (cherry_170) with approximately $2.84\times2.84\times2.84$ mm^3 resolution. We felt that these averaged images would provide comparable texture to our earlier $2.5\times2.5\times2.5$ mm^3 images. Having multiple resolutions within the same species also allowed us to compare classifier accuracy for 2 different image resolutions.

Initial attempts to process yellow poplar images used a 28-12-4 topology for the 3-D ANN, which means that this preliminary classifier had four outputs: clear wood, knots, bark and splits (decay is not present in our yellow poplar images). For yellow poplar logs is which both heartwood and sapwood are present, the classifier performed quite poorly. This occurs because CT image values (density) for heartwood and sapwood are very different. Therefore, it was necessary to distinguish yellow poplar sapwood from the generalized clear wood class (adding an additional classifier output for this class) in order to develop accurate classifiers that used yellow poplar image data.

Using 10-fold cross-validation we developed individual classifiers for each species—red oak, yellow poplar, and cherry—using both 2-D and 3-D feature vectors (6 classifiers). Images used were the nominal $(2.5\text{mm})^3$ resolution. We also

developed multiple-species classifiers: pairing 2 species at a time and combining all 3 species together. These were also trained using 2-D and 3-D feature vectors for a total of 8 multiple-species classifiers. Finally, the finer resolution cherry images $(0.95\text{mm})^3$ were used to train both a 2-D and 3-D classifier.

Table 1. Distribution of training/testing samples taken from different logs and different species. Decay was not present in the yellow poplar samples, and sapwood was not distinguished in the other species.

			Feature type			
Species	**clear wood**	**knots**	**bark**	**splits**	**decay**	**sapwood**
cherry_170	47%	16%	15%	11%	11%	
cherry_512	43%	16%	17%	12%	12%	
red oak	38%	13%	16%	17%	16%	
yellow poplar	46%	15%	15%	5%		19%

4. RESULTS

Classification accuracies for the different classifiers appear in Figure 2. These line plots seem to indicate that 2-D has higher accuracy than 3-D for single-species classifiers, and the reverse performance for multiple-species classifiers. However, it is impossible to determine from these performance estimates whether these apparent differences reflect real accuracy differences. However, because ten-fold cross-validation was used, each trained classifier actually has 10 estimates of classification accuracy, resulting from the accuracy rates from each partition of the data sets. Therefore, these estimates can be used as samples in statistical Analysis of Variance (ANOVA).

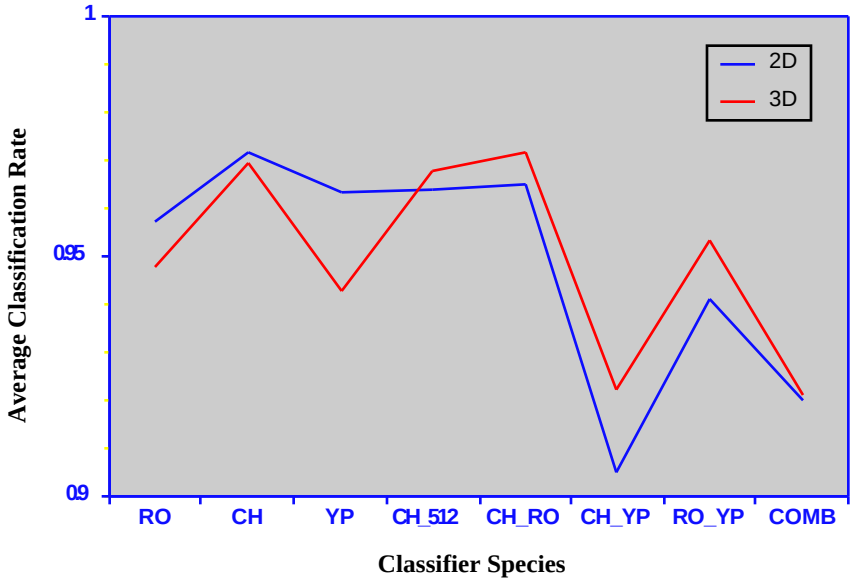

Figure 2. 2-D and 3-D classifier accuracies are plotted for each of the ANN classifiers—red oak (RO), cherry (CH), yellow poplar (YP), 512×512 cherry (CH_512), cherry/red oak (CH_RO), cherry/yellow poplar (CH_YP), red oak/yellow poplar (RO_YP), and all 3 species combined (COMB).

In our first statistical test, we separate the full set of classification rates into two groups: dimensionality which includes two-dimensional and three-dimensional classifiers, and cardinality which includes single (species-dependent) and multiple (species-independent) classifiers. ANOVA treatments, in this case, are single and multiple cardinality, and are blocked on the dimensionality of the classifiers (2-D or 3-D). The F-ratio results for the dimensionality and cardinality are 0.055 (p=0.815) and 27.4 (p<0.001), respectively. It is clear that the F ratio of the dimensionality is much lower than that of cardinality (the former F-ratio is not significant), which indicates (at this point) that differences exist between the mean classification rates for

the single- and multiple-species classifiers. The interaction of dimensionality and cardinality is also significant, indicating a combined effect. This can be seen in the average classification rates of Figure 2, where 2-D rates are generally higher for single-species classifiers and 3-D rates are generally higher for multiple-species classifiers. To determine which means are significantly different for cardinality and dimensionality, post-hoc pair-wise T-tests were performed. The probability values associated with those tests are shown in Table 2. 2-D multiple classifiers have significantly different classification rates from 2-D single and 3-D single classifiers. 2-D single classifiers have significantly different classification rates from 3-D multiple classifiers. 3-D multiple classifiers are not significantly different from 3-D single classifiers.

Table 2. A matrix of pair-wise T-test probability values for different classification rates for various combinations of dimensionality and cardinality.

	2-D multiple	2-D single	3-D multiple	3-D single
2-D multiple	1.000			
2-D single	0.000	1.000		
3-D multiple	0.347	0.001	1.000	
3-D single	0.002	0.301	0.187	1.000

To understand greater details about the differences between dimensionality and cardinality, we performed ANOVAs for single- and multiple-species classifiers separately. For the single-species classifiers, ANOVA treatments are species (CH, RO, and YP) and dimensionality (2-D and 3-D) is used for blocking. F-ratio values for species and dimensionality are 11.4 (p<0.005) and 9.53 (p=0.003), respectively. Probability values associated with post-hoc T-tests are shown in Table 3. They demonstrate that the classification rates for the cherry-specific classifier is significantly different from both those of the red oak- and the yellow poplar-specific classifiers. However, there is no significant difference between the red oak and yellow poplar single-species classifiers.

Table 3. A matrix of pair-wise T-test probability values for the classification rates of cherry, red oak and yellow poplar single-species classifiers.

	CH	RO	YP
CH	1.000		
RO	0.000	1.000	
YP	0.001	0.995	1.000

For the multiple-species classifiers, ANOVA treatments are species (CH_RO, CH_YP, COMB, RO_YP) and dimensionality (2-D and 3-D) is used for blocking. F-ratio values for species and dimensionality are 39.3 (p<0.005) and 4.97 (p=0.032), respectively. Probability values associated with post-hoc T-tests are shown in Table 4. Those values indicate that the CH_RO classifier has significantly greater accuracy than the other 3 multiple-species classifiers. Also, the RO_YP classifier has greater accuracy than the two, lowest accuracy classifiers, COMB and CH_YP. Both of those latter 2 classifiers contain both cherry and yellow poplar samples, which seem to create classification problems. T-tests indicate that COMB and CH_YP are not significantly different from one another.

Table 4. A matrix of pair-wise T-test probability values for the classification rates of cherry, red oak and yellow poplar multiple classifiers.

	CH_RO	CH_YP	COMB	RO_YP
CH_RO	1.000			
CH_YP	0.000	1.000		
COMB	0.000	0.606	1.000	
RO_YP	0.004	0.000	0.000	1.000

Based on the obvious classification problems stemming from combining cherry and yellow poplar samples, we performed our original ANOVA again. This time, treatments were cardinality again, but only CH_RO and RO_YP were included in the multiple-species classifiers (no cherry and yellow poplar combinations). Also, the fine resolution (0.95mm) cherry classifier (CH_512) was excluded from the single-species classifiers. As before, we blocked the ANOVA on dimensionality (2-D and 3-D). The resulting F-ratio value for cardinality is 0.050, which indicates that there is no difference between single- and multiple-species classification rates when cherry/yellow poplar combinations are removed.

Finally, we perform an ANOVA to compare the effect of CT resolution on classifier performance. We eliminated the effect of dimensionality by blocking on it. We found that the finer resolution cherry classifier has no significantly different classification rate over the coarser resolution cherry classifier in our study.

5. SUMMARY AND CONCLUSIONS

This study has empirically investigated a variety of ANN classifiers for defect labeling in CT images of logs. Several species-dependent (single species) and species-independent (multiple species) classifier modules have been developed. Half of the classifiers used 2-D information and half used 3-D information. Classification modules have been tested using CT images from six hardwood logs representing three different species.

The kernel of this automated recognition system is an artificial neural network. For 2-D and 3-D image analysis, there are different numbers of nodes in the first layer of the network corresponding to the local features: features extracted from a 5×5 window for 2-D and from a $3 \times 3 \times 3$ window for 3-D. All of the networks utilize 12 nodes in the middle layer. The number of output nodes varies for different species classifiers. Some classifiers have six nodes and others have five nodes.

Six single-species classifiers were trained using both 2-D and 3-D image data. The accuracy of all 6 classifiers is above 95%. Six, two-species classifiers have also been trained using both 2-D and 3-D image data. Two of them are red oak and yellow poplar combined classifiers, two of them are red oak and cherry combined classifiers, and two are cherry and yellow poplar combined classifiers. Their accuracy is 90%-97%. Finally, combined three-species classifiers (red oak, yellow poplar and cherry) were generated for 2-D and 3-D analysis. These two classifiers identified six kinds of defects: clear wood, knot, bark, split, decay and yellow poplar sapwood. Their accuracy is about 91%-92%.

In comparing 2-D and 3-D features, the performance of 2-D single-species classifiers is better than that of 3-D classifiers. The performance of 3-D multiple-species classifiers is better than that of 2-D classifiers. We conjecture that in single-species classification multiple image planes contain redundant data that may be unimportant, or even counter-productive, for accurate classification. For multiple-species classification, however, the extra information contained in previous and subsequent CT slices seems to aid feature labeling. Consequently, as we increase the species mix that a classifier must deal with, it appears that 3-D features are important for attaining high accuracy.

Higher resolution images do not seem to have a significant difference on performance. We were able to achieve similar accuracies in cherry using ~1mm resolution and ~3mm resolution. This means that our ANN classification approach is general enough to be applied broadly to CT images of varying resolutions. All that is required is resolution-specific training so that the classifier can learn the local neighborhood patterns.

In comparing single-species classifiers and multiple-species classifiers, the performance of the former is better than that of the latter when cherry-yellow poplar combinations are used. On the other hand, when those combinations are excluded, there is no significant difference between classification accuracy for single- and multiple-species classifiers. Yellow poplar has traditionally been difficult to deal with because it possesses many intrinsic differences (wood structure, density) to most other fine-grained hardwoods, e.g., cherry. Yellow poplar was included in the study because it is an extreme case, and we desired to delineate a worst-case scenario. Consequently, the difficulty we experienced in combining it with cherry here is neither surprising, nor particularly worrisome. All of these accuracies (90%-98%) should be acceptable for industrial use. Furthermore, it should be noted that all reported accuracies are *prior* to post-processing. We have visually determined (via classified images) that post-processing does improve accuracy, but we do not have a quantitative estimate for that improvement. Consequently, we expect that the range of accuracies reported above is actual higher, which further enhances its applicability to industrial use.

6. REFERENCES

1. L. G. Occeña, "Computer integrated manufacturing issues related to the hardwood log sawmill," *Journal of Forest Engineering*, Vol. 3, No. 1, pp. 39-45, 1991.
2. D. B. Richards, W. K. Adkins, H. Hallock, and E. H. Bulgrin, "Lumber value from computerized simulation of hardwood log sawing," *U.S. Department of Agriculture, Forest Service, Res. Pap. FPL-356*, Forest Products Lab, Madison WI, 1980.
3. P. H. Steele, T. E. G. Harless, F. G. Wagner, L. Kumar, and F. W. Taylor, "Increased lumber value from optimum orientation of internal defects with respect to sawing pattern in hardwood sawlogs," *Forest Products Journal*, Vol. 44, No. 3, pp. 69-72, 1994.

4. J. A. Tsolakides, "A simulation model for log yield study," *Forest Products Journal*, Vol. 19, No. 7, pp. 21-26, 1969.
5. F. G. Wagner, F. W. Taylor, P. H. Steele, and T. E. G. Harless, "Benefits of internal log scanning," *3rd International Conference on Scanning Technology in Sawmilling*, ed. R. Szymani, Forest Industries/World Wood, San Francisco CA, 1989.
6. F. G. Wagner, T. E. G. Harless, P. H. Steele, F. W. Taylor, V. Yadama, and C. W. McMillin, "Potential benefits of internal-log scanning," *Proceedings of Process Control/Production Management of Wood Products: Technology for the 90's*, pp. 77-88, The University of Georgia, Athens GA, 1990.
7. J. Aune, "The development of a log scanner for sawmills in Canada," *2nd International Seminar on Scanning Technology and Image Processing on Wood*, ed. O. Lindgren, Dept. of Wood Technology, Luleå University, Skellefteå Sweden, 1995.
8. D. M. Benson-Cooper, R. L. Knowles, F. J. Thompson, and D. J. Cown, "Computed tomographic scanning for the detection of defects within logs," *Forest Research Institute, New Zealand Forest Service, Rotorua NZ, Bull. No. 8*
9. R. Birkeland and S. Holoyen, "Industrial methods for internal scanning of log defects: a progress report on an ongoing project in Norway," *2nd International Conference on Scanning Technology in Sawmilling*, ed. R. Szymani, Forest Industries/World Wood, San Francisco CA, 1987.
10. A. E. Burgess, "Potential applications of medical imaging techniques to wood products," *1st International Conference on Scanning Technology in Sawmilling*, ed. R. Szymani, Forest Industries/World Wood, San Francisco CA, 1985.
11. D. J. Cown and B. C. Clement, "A wood densitometer using direct scanning with x-rays," *Wood Science Technol.*, Vol. 17, No. 2, pp. 91-99, 1983.
12. J. R. Davis and P. Wells, "Computed tomography measurements on wood," *Industrial Metrology*, Vol. 2, No. 3/4, pp. 195-218, 1992.
13. A. Grönlund, "Benefits from knowing the interior of the log," *1st International Seminar on Scanning Technology and Image Processing on Wood*, ed. O. Lindgren, Dept. of Wood Technology, Luleå University, Skellefteå Sweden, 1992.
14. S. Grundberg and A. Grönlund, "Log scanning - extraction of knot geometry," *1st International Seminar on Scanning Technology and Image Processing on Wood*, ed. O. Lindgren, Dept. of Wood Technology, Luleå University, Skellefteå Sweden, 1992.
15. T. E. G. Harless, F. G. Wagner, P. H. Steele, F. W. Taylor, V. Yadama, and C. W. McMillin, "Methodology for locating defects within hardwood logs and determining their impact on lumber-value yield," *Forest Products Journal*, Vol. 41, No. 4, pp. 25-30, 1991.
16. F. Hopkins, I. L. Morgan, H. Ellinger, and R. Klinksiek, "Tomographic image analysis," *Materials Evaluation*, Vol. 40, No. 20, pp. 1226-1228, 1982.
17. D. G. Hodges, W. C. Anderson, and C. W. McMillin, "The economic potential of CT scanners for hardwood sawmills," *Forest Products Journal*, Vol. 40, No. 3, pp. 65-69, 1990.
18. L. O. Lindgren, "Medical CAT-scanning: X-ray absorption coefficients, CT-numbers and their relation to wood density," *Wood Science and Technology*, Vol. 25, pp. 341-349, 1991.
19. M. Onoe, J. W. Tsao, H. Yamada, H. Nakamura, J. Kogura, H. Kawamura, and M. Yoshimatsu, "Computed tomography for measuring the annual rings of a live tree," *Nucl. Instrum. Meth. in Physics Res.*, Vol. 221, No. 1, pp. 213-220, 1984.
20. F. Roder, "High speed CT scanning of logs," *3rd International Conference on Scanning Technology in Sawmilling*, ed. R. Szymani, Forest Industries/World Wood, San Francisco CA, 1989.
21. D. L. Schmoldt, "CT imaging, data reduction, and visualization of hardwood logs," *Proceedings of the 1996 Hardwood Research Symposium*, ed. D. Meyer, National Hardwood Lumber Association, Memphis TN, 1996.
22. F. W. Taylor, J. F. G. Wagner, C. W. McMillin, I. L. Morgan, and F. F. Hopkins, "Locating knots by industrial tomography - a feasibility study," *Forest Products Journal*, Vol. 34, No. 5, pp. 42-46, 1984.
23. S. Som, P. Wells, and J. Davis, "Automated feature extraction of wood from tomographic images," *Second International Conference on Automation, Robotics and Computer Vision*, 1992.
24. D. P. Zhu, R. W. Conners, and P. Araman, "CT image sequence processing for wood defect recognition," *the proceedings of the 23rd Southeast Symposium on System Theory*, 1991.
25. B. V. Funt and E. C. Bryant, "Detection of internal log defects by automatic interpretation of computer tomography images," *Forest Products Journal*, Vol. 37, No. 1, pp. 56-62, 1987.
26. D. Zhu, R. W. Conners, D. L. Schmoldt, and P. A. Araman, "CT image sequence analysis for object recognition -- a rule-based 3-d computer vision system," *Proceedings of the 1991 IEEE International Conference on Systems, Man, and Cybernetics*, pp. 173-178, 1991.
27. D. Zhu, R. W. Conners, F. M. Lamb, D. L. Schmoldt, and P. A. Araman, "A computer vision system for locating and identifying internal log defects using CT imagery," *4th Internation Conference of Scanning Technology in Sawmilling*, ed. R. Szymani, Forest Industries/World Wood, San Francisco CA, 1991.

28. D. Zhu, “A Feasibility Study on Using CT Image Analysis for Hardwood Log Inspection” (Ph.D., Virginia Tech University, 1993).
29. P. Li, A. L. Abbott, and D. L. Schmoldt, "Automated analysis of CT images for the inspection of hardwood logs.," *Proceedings of the 1996 IEEE International Conference on Neural Networks*, Institute for Electrical and Electronics Engineers, Inc., Piscataway NJ, 1996.
30. D. L. Schmoldt, P. Li, and A. L. Abbott, “Machine vision using artificial neural networks and 3D pixel neighborhoods,” *Computers and Electronics in Agriculture*, Vol. 16, No. 3, pp. 255-271, 1997.
31. N. Otsu, “A threshold selection method from gray-level histograms,” *IEEE Transactions on Systems, Man, and Cybernetics*, Vol. SMC-9, pp. 62-66, 1979.

PROCEEDINGS OF SPIE

SPIE—The International Society for Optical Engineering

Machine Vision Applications in Industrial Inspection VI

A. Ravishankar Rao
Ning Chang
Chairs/Editors

27 January 1998
San Jose, California

Sponsored by
IS&T—The Society for Imaging Science and Technology
SPIE—The International Society for Optical Engineering

Published by
SPIE—The International Society for Optical Engineering

Volume 3306